Numerical Analysis of Stagger Supersonic Biplane at Off-Design Condition with Trailing Edge Flap

Vijay Kumar Patidar
Associate Professor
Department of Aeronautical Engineering
Parul Institute of Engineering and Technology
Parul University, Vadodara
India

Sudhir Joshi
Professor
Department of Mechanical Engineering
Graphic Era (Deemed to be University)
Dehradun
India

Supersonic biplanes can achieve low-boom and low-drag supersonic flights. In the present study, aerodynamic analysis of a two-dimensional stagger Bussmann biplane (staggered upper element by 0.5c) at zero degrees angle of attack with trailing edge flap was investigated with the help of computational fluid dynamics (CFD) tools. Due to the wave cancellation effect, the Busemann biplane delivers a positive drag reduction at design supersonic Mach values. However, when operating outside of its intended parameters, it performs worse, and the wave cancellation effect has no beneficial effects on reducing drag. Another issue with the Busemann biplane is flow chocking, which produces a potent bow shock wave in front of the aircraft. This paper attempts to address low aerodynamics efficiency problems during take-off through numerical simulation of a staggered Busemann biplane with trailing edge flaps at zero degrees angle of attack. It was confirmed that the staggered biplane airfoil with flap has better aerodynamic performance during take-off at lower subsonic free stream Mach numbers. In 2D wings, the effect of flow chocking and hysteresis as starting problems, which arise when the biplanes accelerate from low Mach numbers, is reduced by using the suitable dimension and angle of rotation of the flap, and the flap is effective in settling these issues.

Keywords: *Supersonic Transport, Busemann biplane, flow choking, shock interaction, sonic boom, flap.*

1. INTRODUCTION

Low noise and high fuel consumptions are critical issues for the next-generation supersonic transport aircraft. A fundamental problem for supersonic transport aircraft is the formation of strong shock waves, and effects are felt on the ground as sonic booms. Even though the first supersonic flight was accomplished in 1947 [1], most supersonic flights to this point have only been con–ducted for military purposes. The only commercial supersonic transport aircraft Concorde was discontinued from operation since 2003 due to its high operational cost, high-frequency sound, and control of the super–sonic flight. High wave drag and sonic boom are the key obstacles to the viability of commercial supersonic tran–sportation. Therefore, a lot of energy is needed to over–come these problems, making supersonic flight very expensive. This is one of the serious problems, and we must overcome it in developing the design of a next-ge–neration supersonic transport aircraft for civil operation.

In 1935, Busemann [2] proposed a biplane confi–guration having the potential that produces low wave drag and low-frequency sonic boom by utilizing favorable shock interaction and reflection between the two elements, as shown in Fig.1. In a supersonic stream, the shock waves between the components interact in such a way as to precisely cancel one another out, which causes the wave drag to occur at a specific Mach number [3].

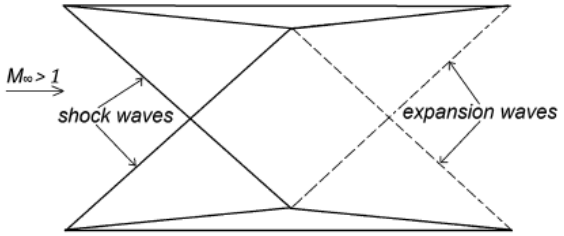

Figure 1. Conceptual the Busemann biplane.

The Busemann biplane is only effective in reducing wave drag under non-lifting conditions at a particular Mach number, however, it shows poor performance, i.e., high wave drag under lifting conditions as well as off-design conditions. Licher studied the Original Busemann biplane and proposed a modified version with varying thicknesses of the lower biplane elements, which is effective at off-design conditions [4]. Recently, a group of scientists at the Japanese Space Exploration Agency (JAXA) has been involved in designing and developing boom-less supersonic aircraft at design Mach number 1.7 [5,6]. Using numerical simulations, they studied the problems encountered in the Busemann biplane at off-design and suggested design modification, successfully reducing the problems encountered in the Busemann biplane [5-8]. Yamashita et al. have sug–gested various methods to overcome the issues of

Received: September 2022, Accepted: April 2023
Correspondence to: Dr Vijay Kumar Patidar
Associate Professor, Department of Aeronautical Engineering, Parul University, Vadodara, Gujrat, India
E-mail- aerovijay112@gmail.com
doi: 10.5937/fme2302253P

choking and hysteresis encountered in Busemann biplane configuration by incorporating leading edge and trailing edge flaps [9]. Kurutani et al. studied the Busemann biplane's stall characteristics and found that the stalling angle of attack is 20˚ for both the upper and lower element of the biplane [10]. They also found that the lower element of the biplane dominates the lift produced and produces a high amount of drag at low subsonic speed and a high angle of attack. The Busemann biplane's flow choking characteristics were researched by Maruyama et al. They suggested com–bining hinged slats and flats to regulate the biplane's intake-to-throat area ratio. They achieved a higher lift-to-drag ratio comparable to a diamond-shaped airfoil [11]. They also indicated that airfoil morphing and Fowler motion might reduce the wave drags on the original Busemann biplane.

When the throat area is smaller than the inlet area for a steady mass flow rate between the biplane elements, flow chocking or beginning problems result. Conversely, to prevent the flow choking characteristics between the biplane parts, the inlet Mach number for a certain area of the throat to the inlet area of the convergent diverging section should be above some defined value indicated by the Kantrowitz limit [12]. Further study is done on the staggered biplane by Vijay Kumar Patidar et al. to enhance the performance characteristics at off-design conditions. Using numerical simulation, they propped staggering of the upper element. The throat-to-area ratio can be controlled and reduces the wave drag at a wide range of subsonic speeds, shown in Fig. 2 [13].

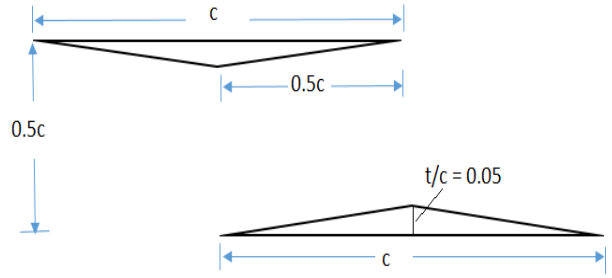

Figure 2. Staggered Busemann biplane.

Even if the staggered biplane controls the flow choking, further research is needed to understand the biplane's flow properties for better supersonic transport aircraft design. The primary goal of the current investigation is to determine how a plain flap (at various flap lengths and flap angles) affects wave drag and aerodynamic effectiveness on a staggered biplane at zero degrees of angle of attack and various Mach values, from low subsonic to supersonic.

The Busemann biplane has an isosceles triangle airfoil and a flat plate in the middle, which replaces the upper isosceles triangle airfoil. Under design conditions, the new supersonic biplane has the same wave-cancellation effect as the Busemann biplane. It also has a weaker flow choking issue in off-design conditions because of a higher ratio of the throat area to the inlet area [17-19].

Although CFD simulation capabilities have ad–vanced significantly in recent years, many complex aerodynamic phenomena still require experimental definition, preferably through wind tunnel testing, because flight testing is too expensive. In addition to its traditional function in aircraft design and performance assessment, one of the main functions of wind tunnel testing in recent years has been providing data for CFD model development and validation. [20-21].

It is extremely challenging to establish precise two-dimensional flow conditions in wind tunnels. This is true for all sizes and types of wind tunnels. The Reynolds number effects of the test model versus the Reynolds number effects of the facility in subsonic and transonic flow are controlled by the influences of the Reynolds number, Mach number, wall interference with reference to solid and flow blockage (blockage of wake), as well as the influence of side-wall boundary layer. [22-23].

The wind tunnel test section's calibration gave researchers insight into the fundamental properties of the flow and how they varied throughout the test section's area. The mean flow variations, Mach number distribution, total and static pressure distribution, and flow angularity, among other flow quality factors, were within the expected ranges. In the test section, the total pressure variation was less than 0.1%, translating to a velocity variation of less than 0.05% [24]. A typical wind tunnel model's configuration is called AGARD-B. It was tested in a wide range of Mach numbers and, more recently, used for the assessment of wall interference effects, validation of computational fluid dynamics codes, and validation of new model produc–tion technologies, in addition to its original intended application for correlation of data from supersonic wind tunnel facilities [25-26].

2. NUMERICAL METHODOLOGY

2.1 Geometric Modelling and Grid Generation

Two half-diamond airfoils with a maximum thickness-to-chord ratio of 0.05 are stacked on top of one another and separated by a gap of 0.5c to form the staggered Busemann biplane. The upper element is placed at a distance 0.5c forward than the lower element, as shown in Fig.2. The subsequent geometry used in the current analysis with trailing edge flaps, as shown in Fig.3. The flap dimension (X) is 0.1, 0.2c and 0.3c are considered with the different flap angles (β) of 10˚, 15˚ and 20˚. ICEMCFD is used to generate all the geometry and grids. The non-staggered elements of the multi-block structured grids have about 0.35 million quadrilateral elements and are saved in an unstructured manner. The grid has a first cell height of 5 x 10^{-6} inside the boundary layer and is stretched perpendicular to the surfaces, in both the longitudinal and lateral directions. The non-dimensional cell wall distance y+ 1 is achieved by setting the initial cell's distance from the wall boundary far enough. When the y+ is greater than 1, mesh adaptation is carried out. The typical mesh around the selected geometry is shown in Fig.4. The number of grids, around 0.35 million, is chosen from extensive grid independence. Studies are performed at a design

Mach number of 1.7. The variation of the drag coefficient with a number of cells is shown in Fig.5.

Adaption of the wall boundary layer impacted the results. Hence accurate prediction of the boundary layer near the solid surface is needed; hence in the current study y++ is calculated based on the flow parameters and incorporated into the solution. [19, 20].

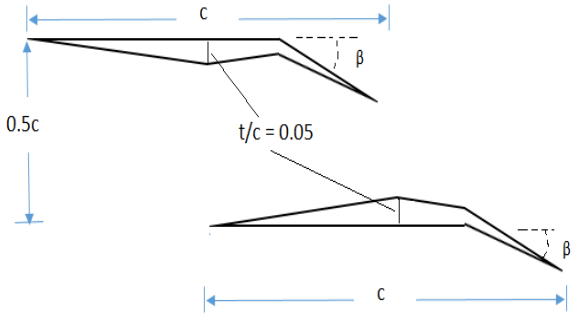

Figure 3. Staggered biplane with Trailing Edge Flaps.

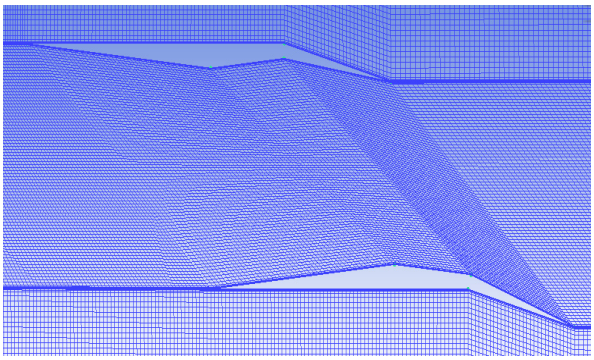

Figure 4. Mesh generation around staggered biplane with trailing edge flaps.

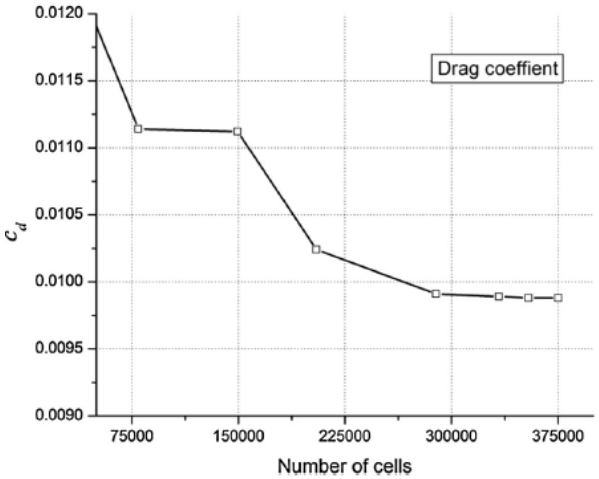

Figure 5. Grid Independent Study of the Busemann biplane at M_∞ = 1.7.

3. METHODOLOGY AND FLOW SOLVER

In earlier days, wind tunnels were the only tool for aerodynamic shape testing and design. In wind tunnels, a part of an aircraft or a complete aircraft, or a scaled model is tested using force and pressure measuring equipment and modified as per design requirements. Wind tunnels are very costly, and data fetching is time-consuming. Nowadays, Computational Fluid Dynamics (CFD) has emerged as a vital tool for aerodynamic design and shape optimization and is widely used in various spectrums of aerodynamic applications. Due to improvements in numerical algorithms and the rapid increase in computer speed and memory, the use of CFD has grown leaps and bounds as approximate results very close to actual values are readily obtained. As this research focuses on the minute geometric variations of the biplane and similar variations of Mach numbers, CFD has been used as the experimentation tool.

Navier-Stokes in two dimensions Equations are linked and solved by ANSYS FLUENT. Modern com–putational fluid dynamics software, such as ANSYS FLUENT, has been successfully validated for internal and external supersonic flows. Strong conservation form for the governing equations over a two-dimensional domain is as follows: [14]

$$\frac{\partial}{\partial t}\int \vec{W} d\Omega + \oint \left(\vec{F}_c - \vec{F}_v\right) dS = \int \vec{Q} d\Omega \tag{1}$$

where,

$$\vec{W} = \begin{bmatrix} \rho \\ \rho u \\ \rho v \\ \rho E \end{bmatrix} \qquad \vec{F}_c = \begin{bmatrix} \rho V \\ \rho u V + n_x p \\ \rho v V + n_y p \\ \rho H V \end{bmatrix}$$

$$\vec{F}_v = \begin{bmatrix} 0 \\ n_x \tau_{xx} + n_y \tau_{xy} \\ n_x \tau_{yx} + n_y \tau_{yy} \\ n_x \Theta_x + n_y \Theta_y \end{bmatrix}$$

where V is the covariant velocity, H is the total ent–halpy, and τ_{xx}, τ_{xy} and τ_{yy} viscous stresses Θ_x, Θ_y represent the work done by the viscous stresses and the heat conduction in respective directions. $\vec{Q}$, represents the vector of the source terms arising due to body forces and volumetric heating.

Sutherland formula and the kinetic theory of gases are used to calculate the variation in molecular viscosity μ and thermal conductivity k of the gases, respectively. The dependent of specific heat of air, Cp, on tempe–rature, is computed using piecewise polynomial approximation. The system of nonlinear equations re–sulting from the discretization of equation (1) over individual control volumes is solved simultaneously in a coupled manner through a point-implicit Gauss-Seidel iterative algorithm in conjunction with the algebraic multigrid method.

4. TURBULENCE MODELLING

Turbulence is the term for fluid particles' uneven, jerky motion that occurs when quantities being conveyed change across time and space. Turbulent modeling is important in the computation of high Reynolds number flows. While performing the simulation, the turbulent models play an important role in the detailed study of turbulent flows. Large-scale turbulence is produced due to the shock-boundary layer interaction and boundary layer separation in the flow field; hence, the correct choice of the turbulence model is necessary for predicting turbulence in the flow field.

In the current work, Reynolds numbers vary from 1.14 x 10^7 to 3.32 x 10^7 for different Mach numbers ranging from 0.5 to 1.4. Under these conditions, the flow is assumed turbulent, and a suitable turbulence model is necessarily required to predict the viscous stresses. The Spalart-Allmaras (S-A) turbulence model predicts turbulence in the flow field. SA turbulence model provides better results in the case of wall-bounded flow, especially in aerospace applications. Like the SA model, the one equation model is a nice middle ground between two-equation models and algebra. For reasonably accurate results at a lower cost for aerodynamic flows, the SA model explicitly solves the transport equation for the eddy viscosity [15]. The reference area has been considered as S = 1 m^2 for the calculations for the biplane configuration.

5. BOUNDARY CONDITIONS

Boundaries are supposed to be characteristic-based pressure far-fields in all directions away from the biplane, where the freestream pressure, Mach number, and static temperature are recorded. The values of the primitive variables are extrapolated from the interior to the downstream pressure far-field boundary. The wall of the biplane is treated as an isothermal boundary condition with an additional no-slip viscous surface with u = v = 0. Moreover, the solution is initialized using the values of the primitive variables at the far-field boundary conditions, as given in Table 1.

Table 1. Far-field boundary conditions

	Symbol	Units	Values
Mach Number	M	-	0.5- 1.4
Temperature	T	K	288.16 K
Pressure	P	N/m^2	101325
Turbulent viscosity ratio	μ_T/μ	-	2.0
Molecular viscosity	μ	Kg/m s	$1.7894x10^{-5}$
Reynolds number	R_e	-	$1.14x10^7 – 3.32x10^7$

6. SOLVER VALIDATION:

Solver validation is done for Diamond and Busemann biplane airfoils by comparing the Drag coefficient and the flow field at non-lifting conditions, i.e., at zero degrees angle of attack. The numerical results are compared with the values reported in the literature and obtained from the shock-expansion theory at design Mach number M_∞ = 1.7, as given in Table 2. A good agreement between the numerical and analytical computations can be seen when comparing the findings shown in Table 2. The presence of viscous stresses, which are not considered in the analytical computations, is the main reason for the variation in the drag coefficient.

Table 2. Theoretical and Numerical results

	Theoretical Results		Numerical results	
	C_l	C_d	C_l	C_d
Diamond airfoil	0.000	0.029	0.000	0.0301
Busemann biplane	0.000	0.000	0.000	0.0099

A comparison is made between the shock wave pattern over the Busemann biplane at various Mach values and those noted in the literature. Figure 6 depicts the pressure coefficient (Cp) contours at different Mach values, from subsonic to supersonic. The Busemann biplane is very similar to the convergent-divergent sec–tion. In the case of low subsonic flow, the inlet to throat area of the section decreases; therefore, the pressure from the inlet to the throat gradually decreases and increases in the downstream part where the throat to exit area increases, this can be seen in Fig. 5a. For High subsonic flow, the flow expands in the convergent section to sonic condition at the throat, and further expansion was observed in the downstream of the section until a normal shock wave formed in the section. This condition leads to the low-pressure area in the latter half part of the section and generates a larger amount of pressure drag. With the further increment in the Mach number, the expansion region increases, and the pressure drag increases. Finally, with an increment in the Mach number, the normal shock wave moved closer to the trailing edge and converted into an attached oblique wave, shown in Fig.5b.

When a biplane element is in a supersonic flow, the flow physics changes, the flow between the biplane elements becomes choked, and a detached bow shock wave forms in front of the biplane elements, changing the flow to subsonic values well head of the biplane configuration (see Fig. 5c). When the Mach number increases, the disconnected shock approaches the components of the biplane and gets stronger. The bow shock wave above and below the biplane becomes more curved as Mach numbers rise, resulting in reduced wave drag than at high subsonic Mach numbers, as seen in Fig. 5d, even if stagnation pressure also rises. The detached shock, still attached to the biplane parts, strikes the corresponding points of maximal thickness at freestream Mach 1.7. Two expansion fans of equal strength emerge at the point of impingement, and the flow continues to expand. As the attached shock waves interact with each other and reduce the strength of the reflected shock and further reduce the strength of expansion waves as the reflected shock interacts with the point of impingement of the expansion waves and reduces the expansion effect and wave drag shown in Fig. 5e.

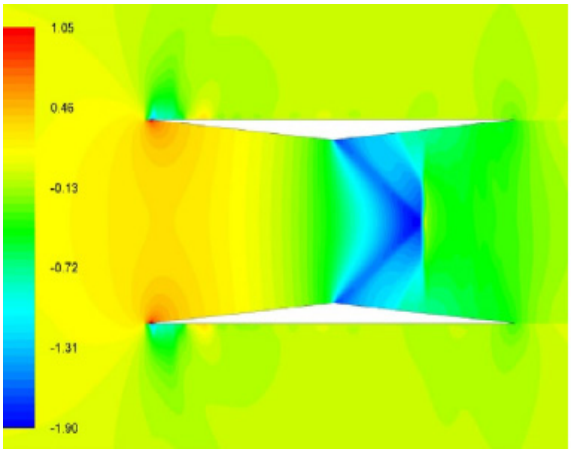

Figure 5(a). M = 0.7

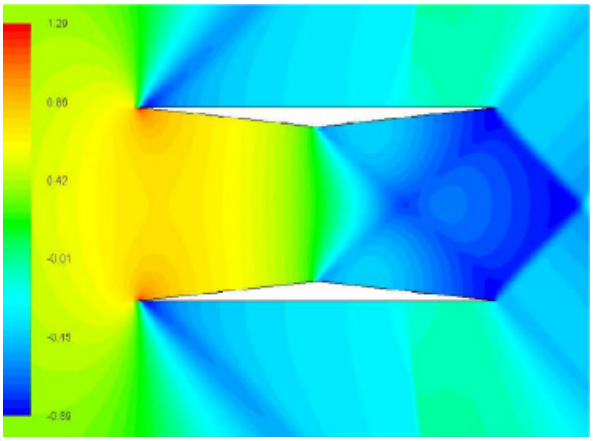

Figure 5(b). M = 1.0

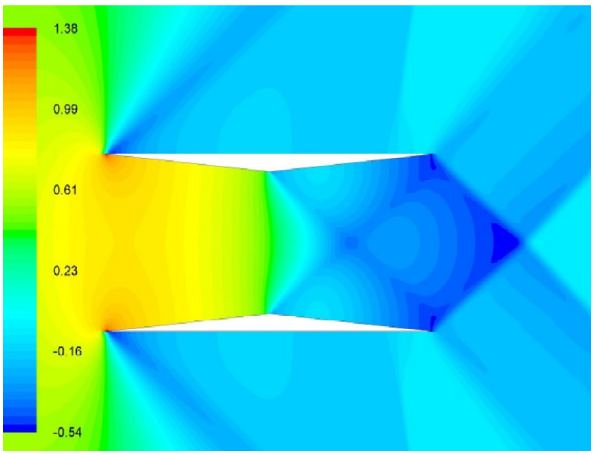

Figure 5(c). M = 1.2

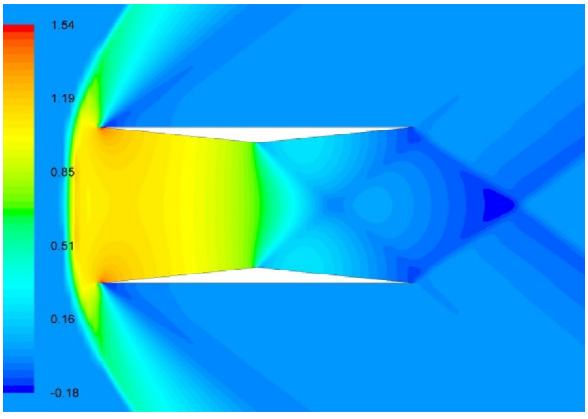

Figure 5(d). M = 1.6

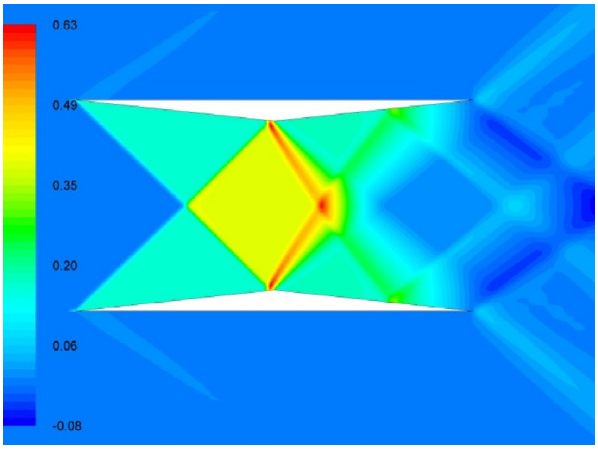

Figure 5(e). M = 1.7

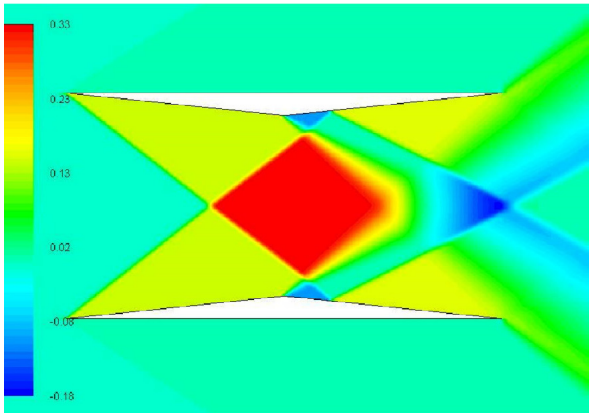

Figure 5(f). M = 1.9

Figure 5. Pressure coefficient contours for the Busemann biplane at different Mach numbers.

The drag variation for the Busemann biplane confi–guration ranging from low subsonic Mach number to supersonic Mach number is shown in Fig.6. The flow field and the drag variation shown in Fig. 5 and Fig. 6 matches well with those reported in the literature for all range of Mach numbers[16].

For the Mach number M_∞>1.7, the attached shock wave angle decreases and the reflected shock wave, not imping at the point of maximum thickness; therefore the flow expansion increases and increases the wave drag shown in Fig. 5f. The pressure distribution remain symmetrical about the horizontal center line of the biplane at all Mach numbers; therefore zero lift distribution is observed.

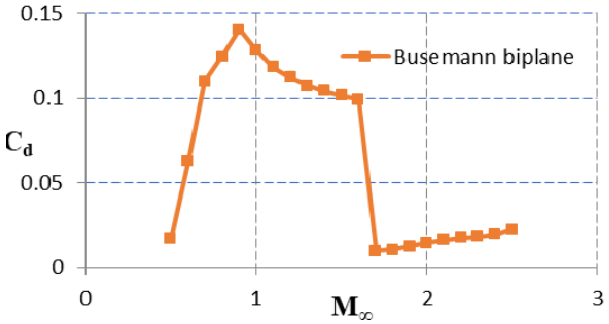

Figure 6. C_d variation with freestream Mach number for the Busemann airfoil at zero-lift condition.

7. RESULTS AND DISCUSSION

At freestream Mach number 1.7, the Busemann biplane shows decent performance, but at freestream Mach number less than 1.7, high wave drag occurs due to the flow chocking between the elements. Staggering the upper element further enhances the performance at subsonic free stream Mach numbers by changing the throat-to-area ratio and controlling the flow chocking phenomena. As the aircraft need to accelerate from a low free stream Mach number, and high value of Lift coefficient or High value of L/D is required during the take-off to fulfill the take-off requirements. The effect of the trailing edge flap has been considered in the present study to enhance the performance of supersonic transport at off-design conditions, i.e., the range of Mach numbers from 0.5 to 1.4.

Staggered upper element by 0.5c in the forward direction used in the current study with the thickness-to-chord ratio of 0.05c; in order to make it simple to com–pare the results with and without the flap condition, the distance between each element and the elements is fixed to 0.5c. The flap dimensions and angle also vary in the current study to understand the variation of lift coefficient and drag coefficient at different Mach numbers.

7.1 Effect of Flap at 0˚ angle of attack

At zero degree angle of attack, the Busemann biplane provides the symmetrical pressure distribution about the horizontal centerline, hence zero lift coefficient, but due to the convergent, divergent section, the pressure dist–ribution is unsymmetrical about the vertical centerline and a large amount of drag coefficient induced by the configuration for the lower value of the free stream Mach numbers (M_∞<1.7).

The staggering upper element will change the throat-to-area ratio; hence, the effect of flow chocking pheno–mena is also reduced, and the pressure is unsymmetrical about both the axis; hence the small amount of positive lift is also provided at lower free stream Mach numbers.

7.2 Effect of flap length 0.1C

At the free stream Mach number 0.5 with a flap length of 0.1c and flap angle of 10 degrees, a high-pressure region is developed below the biplane elements and suction is created in the upper part of both the elements due to the change in the curvature, therefore lift coefficient is increased from 0.1910 to 0.8168, and the drag coefficient is also increased from 0.0170 to 0.0411. The pressure contours with and without the flap are shown in Fig.7.

As the flap angle is increased, i.e., 15˚ and 20˚ at a flap length of 0.1c, the magnitude and the high-pressure region below the elements and the suction on the upper part of the biplane elements increase, therefore increasing the lift and drag coefficient of the biplane configuration. The force components parallel to the flow direction are more due to the increment in the curvature of the elements; therefore increment in drag components is higher than the lift; therefore, Aerodynamic efficiency (L/D) decreases. The variation of pressure coefficient at different flap angles (15˚ and 20˚) at a flap length of 0.1c are shown in Fig. 8.

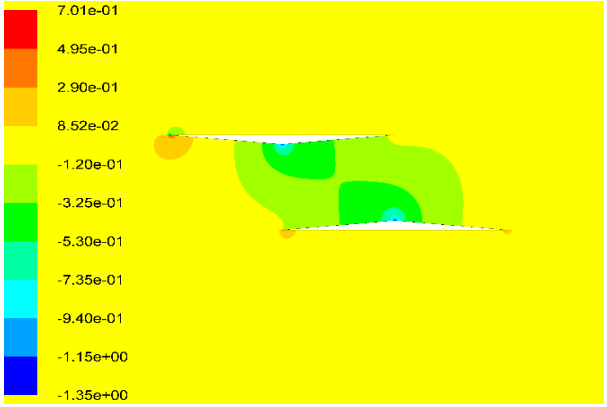

Flap length 0.1c and flap angle 10 degree (C_l =0.1910, C_d= 0.0170)

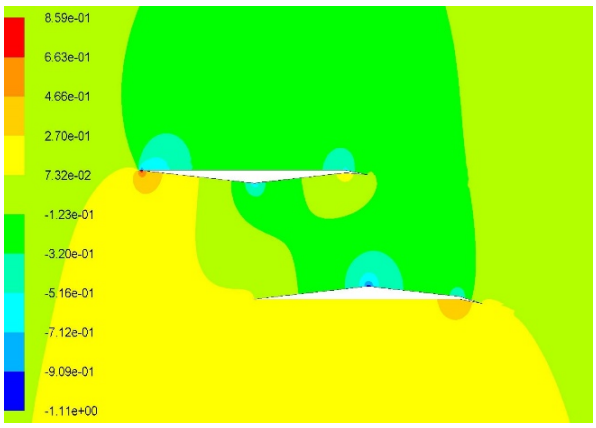

Without flap (C_l = 0.8168 C_d= 0.0411)

Figure 7. Contours of pressure coefficients at M_∞ = 0.5.

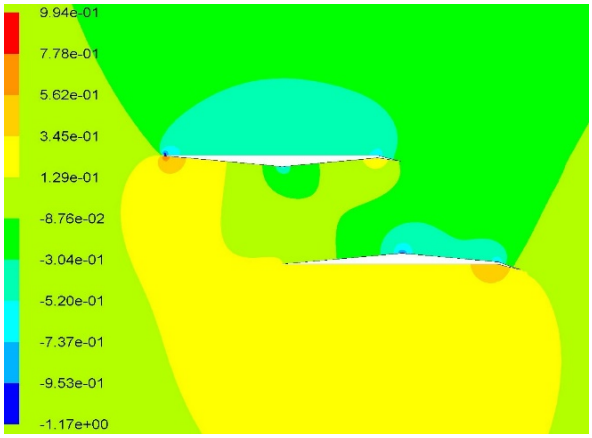

Flap angle 15 degree (C_l =1.0871, C_d = 0.0619)

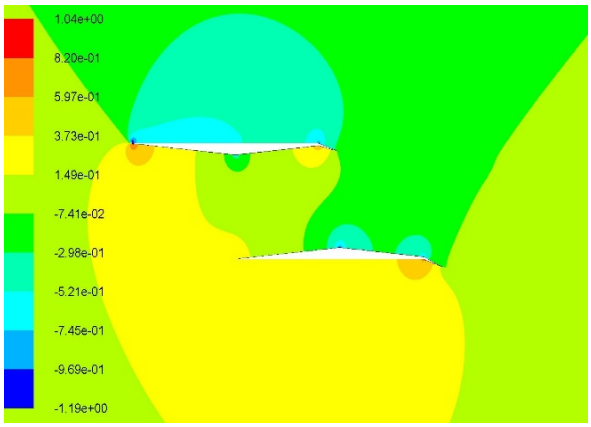

Flap angle 20 degree (C_l = 1.2122, C_d = 0.0814)

Figure 8. Contours of pressure coefficients for flap length 0.1c at M_∞ = 0.5.

For higher subsonic free stream Mach number (M_∞=0.9) at flap length 0.1c and flap angle 10˚, the flow chocking occurs and decreases the flow rate between the elements; therefore, maximum pressure below the biplane elements and the lift coefficient decreases from 0.8168 to 0.7470.

Pressure near the leading edge of the components is quickly increased by flow choking, increasing the drag coefficient from 0.0411 to 0.0866. The shock wave asso–ciated with the top element in the case of supersonic flow (M = 1.4) lowers the pressure along the leading edge of the upper element, lowering the drag coefficient from 0.0886 to 0.0622. At the lower element, the high-pressure

region is developed near the leading edge; therefore, the lift coefficient decreases from 0.7470 to 0.7186. The pressure contours are shown in Fig.9. With the increment in the flap angle (15˚ and 20˚) at flap length 0.1c, the magnitude of the lift coefficient decreases, and the drag coefficient increases. The C_l, C_d, and L/D variation at different free stream Mach numbers is shown in Figure 10.

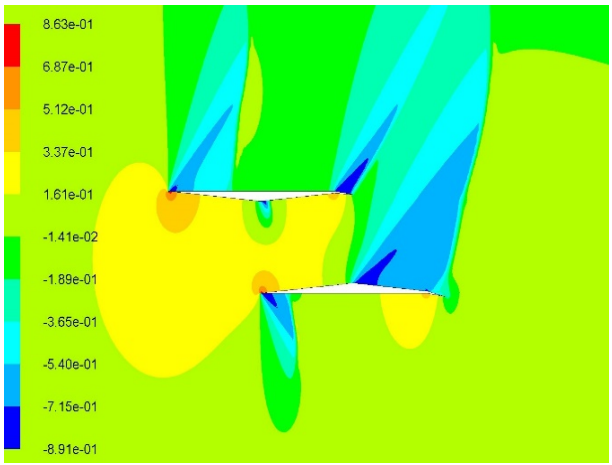

M_∞ = 0.9 (C_l = 0.7470, C_d = 0.0886)

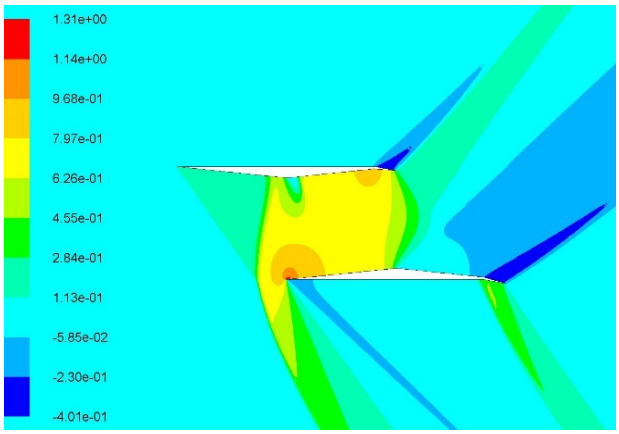

M_∞ = 1.4 (C_l = 0.7186, C_d =0.0622)

Figure 9. Contours of pressure coefficients for flap length 0.1c and flap angle 10˚.

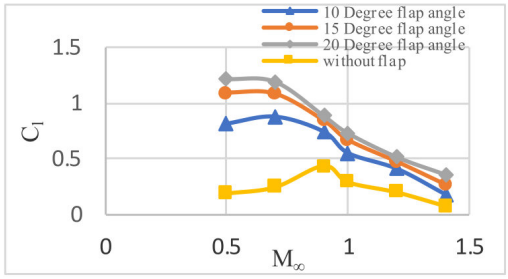

Lift Coefficient

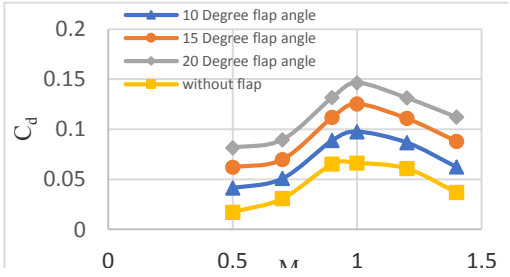

Drag Coefficient

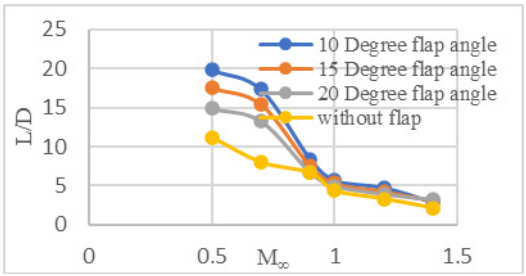

L/D Ratio

Figure 10. C_l, C_d, and L/D ratio variation with free stream Mach number and flap angle at flap length 0.1c.

7.3 Effect of flap length 0.2c and 0.3c

As the flap length increases, the lift and drag coefficient of the biplane increases due to the magnitude of the pressure increasing below the upper element at all flap angles and free stream Mach numbers. The pressure contours at $M\infty$ = 0.5 for different flap lengths are shown in Fig.11, and the variation of L/D ratio is shown in Fig.12. The maximum lift coefficient of 1.9448 and drag coefficient of 0.2215, detected for a flap length of 0.3c and flap angle of 20˚ at a free Mach number of 0.5.

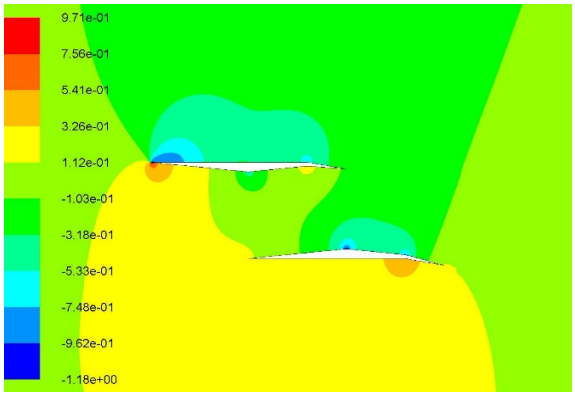

Flap Length 0.2c (C_l = 1.1116, C_d = 0.0639)

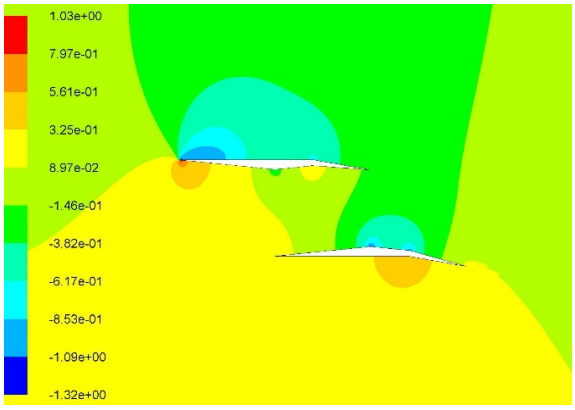

Flap Length 0.3c (C_l = 1.3287, C_d = 0.0871)

Figure 11. Contours of pressure coefficients at M_∞ = 0.5 and flap angle 10˚.

8. CONCLUSION

The effect of the flap on the stagger biplane (upper element forward by 0.5c) on the aerodynamic characteristics is examined numerically for Mach values between 0.5 and 1.4 using a coupled Navier-Stokes solver. The resulting lift and drag coefficient are studied

at various flap lengths (0.1c, 0.2c, and 0.3c) and flap angles (10˚, 15˚, and 20˚) on the staggered biplane and compared the results with no flap condition. It has been observed that the flaps on the staggered biplane signi–ficantly improved the aerodynamic efficiency at all ranges of freestream Mach numbers. The stagger bip–lane's advantage of using flaps is extremely acceptable in the subsonic range when a significant increase in lift coefficient is seen. The maximum lift and drag coef–ficient value is 1.9448, and 0.2215 is detected at a flap length of 0.3c and flap angle of 20˚ at a free Mach number of 0.5. Although the Maximum Aerodynamics efficiency was found as 19.86 at flap length 0.1c and flap angle 10˚ at a free stream Mach number 0.5.

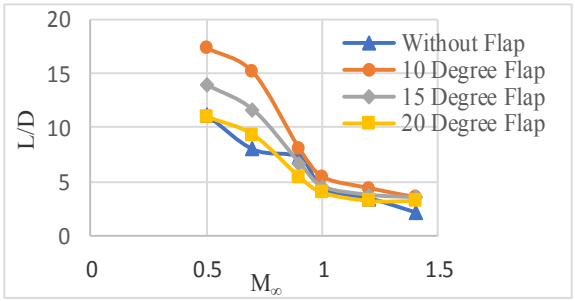

Flap length 0.2c

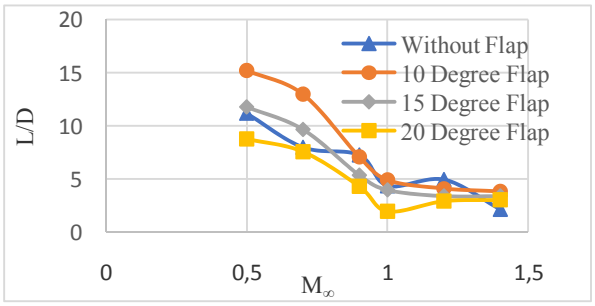

Flap length 0.3c

Figure 12. L/D ratio variation with free stream Mach number.

Incorporating flaps on both elements helps the supersonic transport meet the take-off and landing requirements where large values of lift and drag coef–ficient are necessary at low subsonic free stream Mach numbers, as opposed to the stagger biplane, which per–forms well at off-design conditions over the standard Busemann biplane. Based on the lift and drag calcu–lations for the three-dimensional wing with different configurations of other geometric factors, the ultimate compromise to choose the flaps' span may be made.

REFERENCES

[1] J.D. Anderson, *Introduction to Flight*, McGraw Hill, 2005.

[2] Busemann, A. Aerodynamic lift at supersonic speeds, *Proc. Volta Congress,* 315–347 or *Luftfahrtforshung,* Vol. 12, 210–220, 1935.

[3] H.W. Liepmann, A. Roshko, *Elements of Gas Dynamics,* John Wiley & Sons, Inc., 1957.

[4] R.M. Licher, Optimum two-dimensional multiplanes in supersonic flows, Report, No. SM-18688, Douglas Aircraft Co., 1955.

[5] K. Kusunose, A new concept in the development of boomless supersonic transport, in: *First International Conference on Flow Dynamics, Sendai, Japan,* November 2004.

[6] K. Kusunose, K. Matsushima, Y. Goto, H. Yamashita, M. Yonezawa, D. Maruyama, T. Nakano, A fundamental study for the development of boomless supersonic transport aircraft, AIAA Paper, AIAA-2006-0654, January 2006.

[7] D. Maruyama, K. Matsushima, K. Kusunose, K. Nakahashi, Aerodynamic design of biplane airfoils for low wave drag supersonic flight, in: *The 24th Applied Aerodynamic Conference, San Francisco*, 2006.

[8] Kisa Matsushima, Kazuhiro Kusunose, Daigo Maruyama, Takumi Matsuzawa, Numerical design and assessment of a biplane as future supersonic transport, in: *Proceedings of the 25th ICAS Congress,* 3.7.1, pp. 1–10, 2006

[9] H. Yamashita, M. Yonezawa, S. Obayashi, K. Kusunose, A study of Busemann type biplane for avoiding choked flow, *AIAA Paper*, AIAA2007-0688, 2007.

[10] Naoshi Kuratani, Shuichi Ozaki, Shigeru Obayashi, Toshihiro Ogawa, Takashi Matsuno, Hiromitsu Kawazoe, Experimental and computational studies of low-speed aerodynamic performance and flow characteristics around a supersonic biplane, Trans. Jpn. Soc. Aeronaut. Space Sci. 52 (176), 89–97, 2009

[11] Daigo Maruyama, Kazuhiro Kusunose, Kisa Matsushima, Aerodynamic characteristics of a two-dimensional supersonic biplane, covering its take-off to cruise conditions, Shock Waves Vol. 18, 437–450, 2009

[12] Van Wie, D.M., Kwok, F.T and Walsh, R.F., Starting characteristics of supersonic inlets, *AIAA Paper*, 2914. 1996.

[13] Vijay Kumar Patidar, Rajesh Yadav, Sudhir Joshi, Numerical investigation of the effect of stagger on the aerodynamic characteristics of a Busemann biplane, Aerospace Science and Technology Vol. 55, pp. 252–263, 2016

[14] Blazak K. *Computational Fluid Dynamics: Principles and Applications*, second edition, Elsevier, ISBN-13:978-0-08-044506-9, 2005.

[15] Spalart P. R., & Allmaras SRA). One-equation turbulent model for aerodynamic flows. *AIAA Paper, American Institute of Aeronautics and Astronautics*, 92, pp. 0439, 1992.

[16] H. Yamashita, N. Kuratani, M. Yonezawa, T. Ogawa, H. Nagai, K. Asai, S. Obayashi, Wind tunnel testing on start/unstart characteristics of finite supersonic biplane wing, *Int. J. Aerosp. Eng.* 231434, 2013.

[17] Jian Zhai, Chen-An Zhang, Fa-Min Wang, Wei-Wei Zhang, Design of a new supersonic biplane, Acta Astronautica 175 (2020) 216-233.

[18] K Yu, J. Xu, S Liu, X Zhang: Starting characte–ristics and phenomenon of a supersonic wind tunnel coupled with inlet model, Aero. Sci. Technol. 77 (2018) 626-637.

[19] S J Hu, Z X Sun, G W Yang, P Prapamonthon, J Y Zhang, Parametric study on drag reduction with the combination of the upstream energy deposition and the opposing jet configuration in supersonic flows, Acta Astronaut. 171 (2020) 300-310.

[20] Damljanovic, D., Vukovic, Đ., Ocokoljic, G., Ilic B, Rasuo, B.: Wind Tunnel Testing of ONERA-M, AGARD-B, and HB-2 Standard Models at Off-Design Conditions, Aerospace, Vol.8(10), 275; 2021.

[21] Kostic, C., Bengin, A., Rasuo, B., Damljanovic, D.: Calibration of the CFD Code Based on Testing of a Standard AGARD-B Model for Determination of Aerodynamic Characteristics. Proc. Inst. Mech. Eng. Part G J. Aerosp. Eng. 2021, Volume 235, pp. 1129–1145.

[22] Rasuo, B.: Scaling between Wind Tunnels–Results Accuracy in Two-Dimensional Testing, Transactions of the Japan Society for Aeronautical & Space Sciences, Vol.55, No.2, March 2012, pp. 109-115.

[23] Rasuo, B.: The influence of Reynolds and Mach numbers on two-dimensional wind-tunnel testing: An experience, The Aeronautical Journal, Volume 115, Number 1166, Paper No. 3542, 2011, pp. 249-254.

[24] Ocokoljic, G., Damljanovic, D., Vukovic, D., Rasuo, B.: Contemporary Frame of Measurement and Assessment of Wind-Tunnel Flow Quality in a Low-Speed Facility, FME Transactions, 46 (4): pp. 429-442, 2018.

[25] Damlanovic, D., Vukovic, Dj., Ocokoljic, G., Rasuo, B.: Convergence of transonic wind tunnel test results of the AGARD-B standard model, FME Transactions, Vol. 48, No. 4, pp. 761-769, 2020.

[26] Ocokoljic, G., Damljanovic, D., Rasuo, B., Isakovic, J.: Testing of a standard model in the VTI's large-subsonic wind-tunnel facility to establish users' confidence, FME Transactions 42 (3), pp. 212-217, 2014.

НУМЕРИЧКА АНАЛИЗА ТЕГЉАЈУЋЕГ НАДЗВУЧНОГ ДВОКРИЛЦА У УСЛОВИМА ВАН ПРОЈЕКТОВАЊА СА ЗАКЛОПКОМ ЗАДЊЕ ИВИЦЕ

В.К. Патидар, С. Џоши

Надзвучни двокрилци могу да остваре надзвучне летове са ниским стрелом и малим отпором. У овој студији, уз помоћ алата за рачунарску динамику флуида (ЦФД) истражена је аеродинамичка анализа дводимензионалног тегљајућег Бусмановог дво–крилног авиона (помакнут горњи елемент за 0,5ц) при нападном углу од нула степени са преклопом задње ивице. Због ефекта поништавања таласа, Бусманнов двокрилац показује позитивно смањење отпора при пројектованим суперзвучним Маховим вредностима. Међутим, када ради ван предвиђених параметара, ради се лошије, а ефекат поништавања таласа нема благотворно дејство на смањење отпора. Још један проблем са двокрилним авионом Бусманн је гушење протока, које производи снажан прамчани ударни талас испред авиона. Овај рад покушава да се позабави проблемима ниске аеродинамичке ефикасности током полетања кроз нумеричку симулацију распоређеног Бусмановог двокрилца са закрилцима задње ивице под нападним углом од нула степени. Потврђено је да распоређени двокрилни аеропрофил са преклопом има боље аеродинамичке перформансе током полетања при нижим Маховим бројевима слободног тока под–звучног тока. У 2Д крилима, ефекат гушења протока и хистерезе као почетних проблема, који настају када двокрилци убрзавају са ниских Махових бројева, смањен је коришћењем одговарајуће димензије и угла ротације преклопа, а преклоп је ефикасан у решавању ових проблема.